COMPARISON OF THE SIZE EFFECT PREDICTED BY A COHESIVE ZONE MODEL AND THE FINITE FRACTURE MECHANICS FOR THE FIBER-MATRIX DEBONDING

I. G. García*[1], M. Paggi[2], V. Mantič[1]

[1] *Grupo de Elasticidad y Resistencia de Materiales, Escuela Técnica Superior de Ingeniería, Universidad de Sevilla, Camino de los Descubrimientos s/n, 41092 Sevilla, Spain*
[2] *IMT Institute for Advanced Studies Lucca, Piazza San Francesco 19, 55100 Lucca, Italy*
* *Corresponding Author: israelgarcia@us.es*

Keywords: fiber-matrix interface debonding, cohesive zone model, finite fracture mechanics, size effect

Abstract
The fiber-size effects on the value of the homogenized transverse stress leading to the onset of crack initiation at the fiber-matrix interface predicted by the cohesive zone model and by the finite fracture mechanics theory are herein compared and discussed. The results show a good agreement except for the limit cases corresponding to small or very large fibers. The causes for the observed differences are analyzed and explained by means of simplified asymptotic models.

1. Introduction

Fiber-matrix debonding under transverse tension has been studied for decades due to its responsibility in the failure mechanism known as inter-fiber or matrix failure in composites. It is well known, see e.g. [1], that this failure mechanism starts with small cracks at the fiber-matrix interface or near it. Subsequently these cracks grow along the interface to finally kink out the interface toward the matrix, coalescing with other cracks. The first part of the process, the crack initiation at the fiber-matrix interface has been studied recently from the point of view of several theoretical and computational approaches, see e.g. [2–5]. One of the most interesting results found by these analyses is the fiber-size effect on the critical transverse tension necessary for the crack initiation at the fiber-matrix interface.

This work aims at comparing the fiber-size effect predicted by two models which have been recently proposed to study the problem of crack initiation at the fiber-matrix interface. The first model [2] assumes that the interface behavior can be approximated by a cohesive law which is very common in models dealing with crack initiation. The second model [3] is based on the coupled criterion [6] of the finite fracture mechanics [7, 8] which predicts that a crack of finite extension appears abruptly when the following two conditions are fulfilled: i) the stresses along the future crack surface exceeds a critical value and ii) the onset of the crack is energetically allowed.

As an example, both models are applied to the composite studied in [2] and the results obtained

	Young's modulus (GPa), E_i	**Poisson's ratio.** ν_i
fiber (f)	340	0.18
matrix (m)	60	0.3

Table 1. Elastic properties of the composite.

are compared. Both constituents, fiber (f) and matrix (m), are assumed to be linear elastic and isotropic materials with the elastic properties shown in Table 1.

First, the formulation of each model is described in Section 2 including all the parameters necessary to set the models. The results obtained by the two formulations are presented and compared in Section 3. Finally the results of the comparison are discussed in Section 4 giving an interpretation to the asymptotic behavior found for large and small fibers.

2. Models

This section describes briefly the aforementioned models subject of the study with a special emphasis on the characteristics and the parameters which are shared by the two models. In this sense the model based on the coupled criterion proposed in [3] is slightly modified to be more coherent with the cohesive law used in [2].

2.1. Cohesive zone model

Cohesive zone models (CZM) are widely used to approximate the progressive nonlinear behavior of the fracture process by assuming a cohesive law of separation between the fracture surfaces [9]. CZM enable to avoid two classic problems of the linear elastic fracture mechanics: i) CZM avoid the stress singularity at the crack tip and ii) CZM are able to predict crack initiation. In the model described here, this is used to simulate the progressive debonding at the fiber-matrix interface.

The problem is studied by employing a plane strain model in the plane perpendicular to the fiber axis. The unit cell is represented in Figure 1(a): a circular inclusion with radius a corresponding to the fiber is surrounded by a square with side b corresponding to the matrix. The simulations are carried out for several values of the radius. In order to avoid the influence of the volumetric fraction v, the ratio $b/a = 4.18$ which corresponds to $v = 18\%$ is fixed for all the simulations, see [10] for a discussion on the influence of v. A normal displacement δ and vanishing shear stresses are prescribed at the two vertical external boundaries of the unit cell, whereas the horizontal external boundaries are free. The value of δ is increased monotonically. A homogenized longitudinal strain ε_1 is defined as,

$$\varepsilon_1 = \frac{2\delta}{b} \tag{1}$$

Analogously, a homogenized stress σ_1 is defined as the mean value of the normal stresses at the external boundary where the displacement δ is prescribed.

The interface behavior is modeled by means of the cohesive law proposed in [11]. According to this law, the normal σ and shear τ interface stresses are functions of the relative normal g_{N}

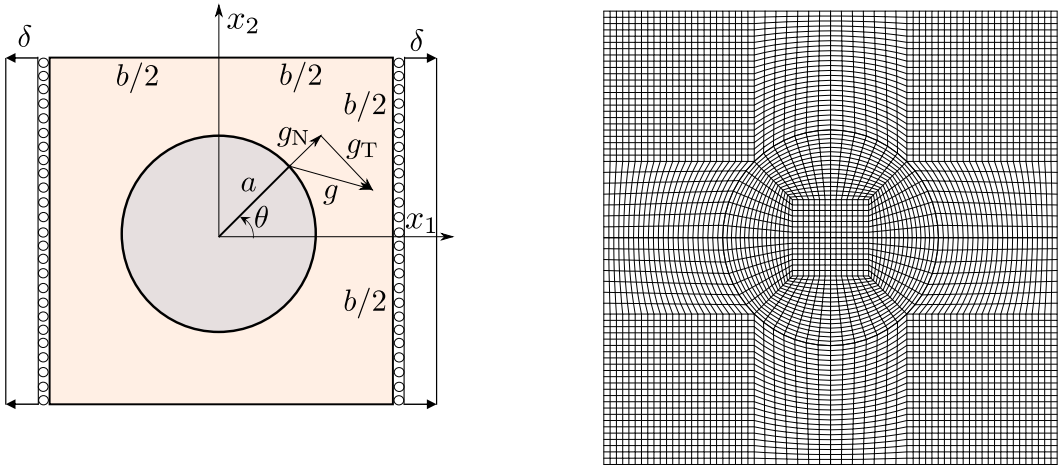

(a) (b)

Figure 1. Schematic of the CZM simulation: (a) geometry and boundary conditions and (b) mesh

and tangential g_T displacements at the interface,

$$\sigma = \sigma_c \frac{g_N}{l_{Nc}} P(\lambda) \tag{2a}$$

$$\tau = \tau_c \frac{g_T}{l_{Tc}} P(\lambda) \tag{2b}$$

with

$$P(\lambda) = \begin{cases} \dfrac{27}{4}(1-\lambda)^2, & \text{for } 0 \le \lambda \le 1 \\ 0, & \text{otherwise} \end{cases} \qquad \text{and} \qquad \lambda = \sqrt{\left(\frac{g_N}{l_{Nc}}\right)^2 + \left(\frac{g_T}{l_{Tc}}\right)^2}. \tag{3}$$

where σ_c and τ_c are respectively the interface tensile and shear strengths. l_{Nc} and l_{Tc} are the critical relative normal and tangential displacements respectively. In addition, $g_N \ge 0$ is forced to avoid interpenetrations along the interface. Figure 2 shows the shape of this cohesive law. Observe the great interaction between the modes prescribed by this cohesive law. For the sake of illustration the next values are taken: $\sigma_c = \tau_c = 300$ MPa and $l_{Nc} = l_{Tc} = 0.03$ μm.

The resulting nonlinear problem presented in Figure 1(a) is solved numerically by employing the finite element (FE) code FEAP. The model is discretized using standard 2D plane strain elements with quadratic shape functions, see Figure 1(b). The curvilinear interface is discretized applying the *virtual node technique* [12, 13]. The kinematic variables g_N and g_T are determined using a node-to-segment strategy. Depending on the sign of g_N, an automatic switching procedure is adopted to change between contact and cohesive model for the normal direction at the interface. In the case of negative g_N, a penalty formulation is implemented to enforce $g_N \ge 0$.

2.2. Finite fracture mechanics: coupled criterion

The coupled criterion [6], proposed in the context of the finite fracture mechanics (FFM) [7, 8], is based on two key ideas. The first is common to all the approaches in FFM: a crack onset of a finite extension is predicted. The second is the assumption referred to as Leguillon's hypothesis: the crack onset requires the simultaneous fulfillment of a stress and an energy criterion.

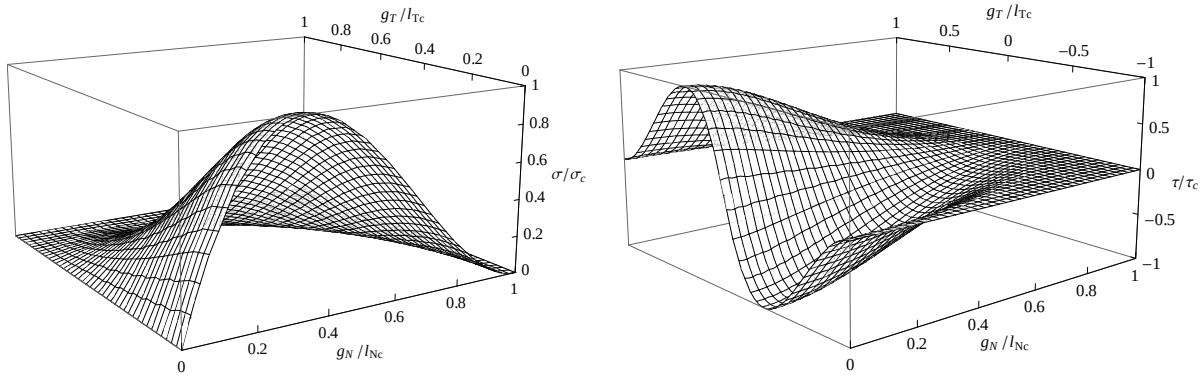

(a) Normal cohesive stresses (b) Tangential cohesive stresses

Figure 2. Tvergaard CZM law used to describe the progressive debonding process of the fiber-matrix interface.

The two linear elastic states studied in the FFM model proposed in [3] are shown in Figure 3. Similarly to the model presented in previous section, a plane strain analysis in the plane perpendicular to the fiber axis is employed. Thus, a circular inclusion with radius a surrounded by an infinite matrix is modeled. Note that, on the contrary to the CZM, the matrix here is unbounded. The reason is that this enables to build a model exclusively based on analytical solutions which are available in the literature for an infinite matrix. This difference between both models is not supposed to introduce a relevant disagreement in the results as shown in [10]. A remote tension σ_1 is applied. According to the FFM model, the fiber-matrix interface is initially perfectly bonded. σ_1 is monotonically increased up to a critical value σ_{1c} for which both criteria studied later on are fulfilled. Then, a crack of a finite extension with polar semiangle $\Delta\theta$ appears abruptly, see Figure 3(b). In what follows, the condition imposed by both criteria for this particular problem is briefly developed.

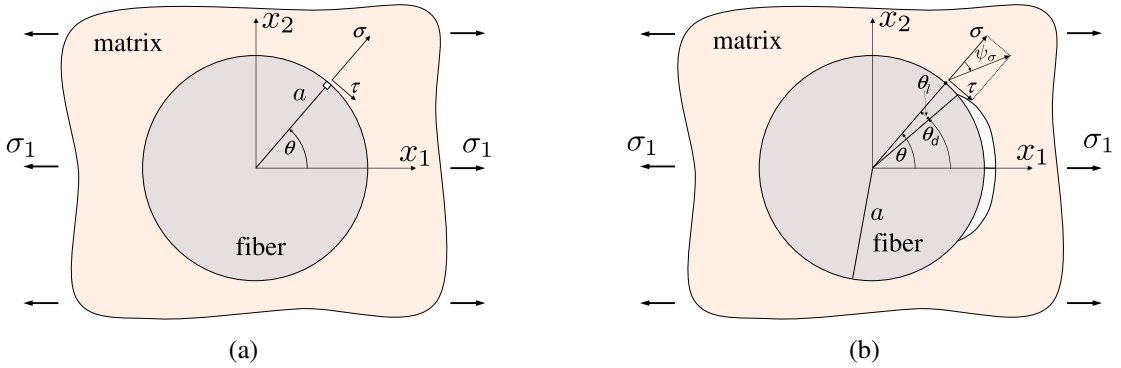

(a) (b)

Figure 3. Schematic of the situation assumed by the FFM model (a) before and (b) after the interface crack onset.

The stress criterion employed imposes that the stresses at the points of the interface where the crack will appear has to be equal or larger than a critical value. The model in [3] utilized a tensile stress criterion based exclusively on the normal stresses. However, due to the influence of the shear stresses in the cohesive law, a Mohr-Coulomb stress criterion is proposed for this

comparison. Thus, the stress criterion writes as

$$\sigma_{\mathrm{eq}}(\theta) = \sigma(\theta) + \frac{\tau(\theta)}{\tau_{\mathrm{c}}/\sigma_{\mathrm{c}}} \geq \sigma_{\mathrm{c}}, \ \forall \theta \in [0, \Delta\theta], \tag{4}$$

where θ is the polar angle at the interface and $\sigma(\theta)$ and $\tau(\theta)$ are, respectively, the normal and shear interface stresses prior to the crack onset, see Figure 3(a). An analytical solution for $\sigma(\theta)$ and $\tau(\theta)$ is available in [14]. Taking into account that $\sigma(\theta)$ and $\tau(\theta)$ are proportional to σ_1 and under the assumption that the pole $\theta = 0°$ is always included in the onset, the stress condition in (4) can be rewritten as,

$$\frac{\sigma_1}{\sigma_{\mathrm{c}}} \geq s(\Delta\theta, \alpha, \beta, \tau_{\mathrm{c}}/\sigma_{\mathrm{c}}) \tag{5}$$

where the function s is analytical and can be obtained from the expressions of $\sigma(\theta)$ and $\tau(\theta)$, see [10]. α and β are the Dundurs bimaterial elastic parameters, see [3] for their expressions.

The energy criterion is based on an incremental energetic balance. Assuming a quasi-static initial state, the energetic balance can be written as,

$$-\Delta\Pi \geq \Delta\Gamma \tag{6}$$

where $\Delta\Pi$ is the change in elastic potential energy and $\Delta\Gamma$ is the dissipated energy during the fracture process. $\Delta\Pi$ can be approximated by the integration of the energy release rate G since $G = -\mathrm{d}\Pi/2a\mathrm{d}\theta$. An analytical expression for G was obtained in [15] and can be written as $G(\theta_{\mathrm{d}}, \sigma_1, a, E_{\mathrm{f}}, \nu_{\mathrm{f}}, E_{\mathrm{m}}, \nu_{\mathrm{m}}) = \sigma_1^2 a \hat{G}(\theta_{\mathrm{d}}, \alpha, \beta)/E^*$, see [3] for an expression of the dimensionless energy release rate $\hat{G}$, E^* is the harmonic mean of the effective Young's moduli. Regarding to $\Delta\Gamma$, it is approximated in [3] by the integration of the interface fracture toughness which depends on the fracture mode mixity. In the CZM, $\sigma_{\mathrm{c}} = \tau_c$ and $l_{\mathrm{Nc}} = l_{\mathrm{Tc}}$ which corresponds to a fracture toughness independent of the mixity as demonstrated in [10]. In order to be coherent with the CZM employed, the dissipated energy is directly approximated by $\Delta\Gamma = G_{1\mathrm{c}} 2a\Delta\theta$ where $G_{1\mathrm{c}}$ is the interface fracture toughness in pure mode 1. Finally, the energetic balance in (6) can be rewritten in an analogous manner to the stress criterion as,

$$\frac{\sigma_1}{\sigma_{\mathrm{c}}} \geq \sqrt{\frac{G_{1\mathrm{c}} E^*}{\sigma_{\mathrm{c}}^2 a} g(\Delta\theta, \alpha, \beta)} \tag{7}$$

where $g(\Delta\theta, \alpha, \beta) = \Delta\theta / \int_0^{\Delta\theta} \hat{G}(\theta_{\mathrm{d}}) \mathrm{d}\theta_{\mathrm{d}}$.

Once the expressions of the conditions corresponding to the two criteria are known, Leguillon's hypothesis postulates that the critical remote stress $\sigma_{1\mathrm{c}}$ is given by the minimum value of σ_1 fulfilling both criteria. Hence,

$$\frac{\sigma_{1\mathrm{c}}}{\sigma_{\mathrm{c}}} = \min_{\Delta\theta \in [0°, 90°]} \left(\max \left[s(\Delta\theta, \alpha, \beta, \tau_{\mathrm{c}}/\sigma_{\mathrm{c}}), \ \sqrt{\frac{G_{1\mathrm{c}} E^*}{\sigma_{\mathrm{c}}^2 a} g(\Delta\theta, \alpha, \beta)} \right] \right). \tag{8}$$

where the values of all the parameters have been defined except for the value for $G_{1\mathrm{c}}$, which can be obtained by integrating the cohesive law giving $G_{1\mathrm{c}} = 5.0625$ J/m^2, see [10].

3. Results

The nonlinear model with CZM is solved for several values of the fiber radius. The stress-strain curves obtained from the simulations show that for large fibers, a maximum for σ_1 is observed leading to a snap-back instability, see [10] for a detailed exposition of the curves and a subsequent discussion. The value of this maximum is identified with the critical value σ_{1c}. However, below a certain value of the fiber radius, the stress-strain curves do not have a maximum but they have a change of tendency in the form of an inflection point which is taken as reference for the value of σ_{1c}.

In the case of the FFM model, a curve of σ_{1c} as a function of a is calculated through the expression (8) for a sufficiently wide range of fiber radii.

The results predicted for σ_{1c} for each model are represented in Figure 4. The threshold value for the fiber radius separating the results of the CZM corresponding to a maximum or an inflection point on the stress-strain curve is indicated. For FFM, the solid line corresponds to the expression given by (8). Observe that two horizontal asymptotes as dashed lines have been represented for the FFM model in the case of large fibers. The upper one corresponds to the asymptote of the expression (8). The lower one is calculated by relaxing the hypothesis of crack onset including $\theta = 0°$. As demonstrated in [3], the stress criterion governs the asymptote for large fibers. Since the Mohr-Coulomb criterion used here predicts that the most critical point is not situated at $\theta = 0°$, the rigorous asymptote is the lower one, see [10] for a detailed discussion.

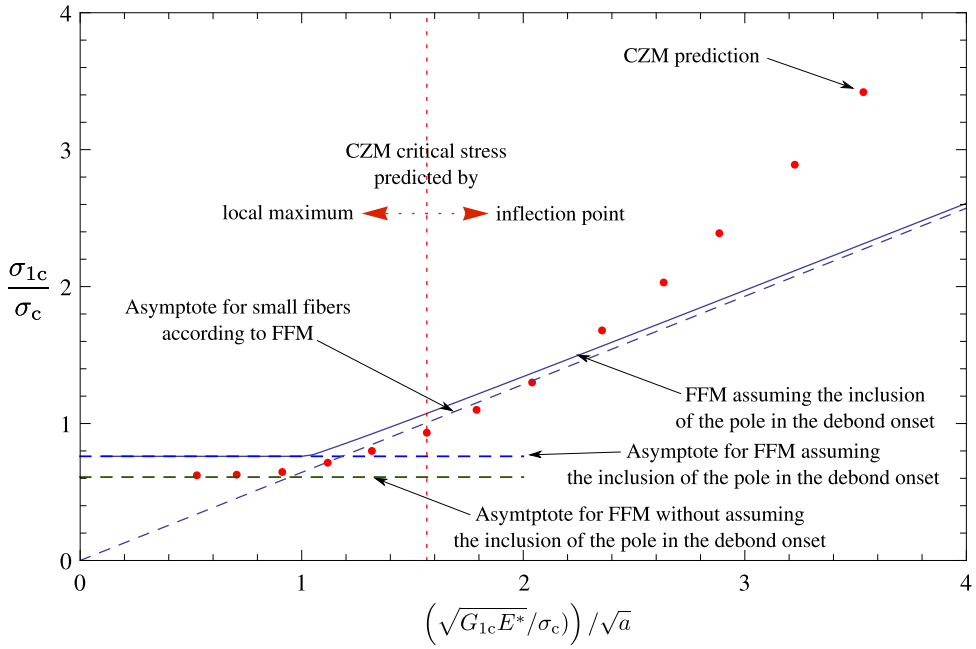

Figure 4. Comparison of the results predicted for the critical tension σ_{1c} by the CZM and the coupled criterion of the FFM as a function of the fiber radius a.

4. Discussion

Figure 4 shows a moderate agreement between the results predicted by CZM and FFM. This agreement is better for large and medium fibers than for small fibers where the values diverge

considerably. The difference in the agreement and tendency for large and small fibers can be explained by asymptotic models briefly presented in the following, see [10] for a full discussion.

For large fibers, σ_{1c} in the FFM model is governed by the stress criterion as has been highlighted by several authors, see e.g. [3]. In the case of CZM, when the fiber radius increases, the stiffness of the cohesive elements increases with respect to the global stiffness of fiber and matrix as shown in [10]. As a consequence, the stress solution in CZM tends to the solution given by a perfectly bonded interface, i.e. the solution used in the FFM for the evaluation of the stress criterion. This explains why the agreement between models is excellent for large fibers. In addition, since the stress solution of the asymptotic model is independent of the fiber radius (with v fixed), the results tend to a horizontal asymptote.

For small fibers, the FFM model is governed by the energy criterion which predicts σ_{1c} is proportional to $1/\sqrt{a}$ [3], which corresponds to a linear behavior in Figure 4. The tendency of the CZM results can be interpreted with an asymptotic model analogous to that used previously for large fibers. When the fiber radius decreases, the relative stiffness of the cohesive elements with respect to the fiber and matrix stiffness decreases. In the limit, the model tends to have the stresses and displacements of a model with the fiber-matrix interface totally debonded [10]. Thus, the relative normal and tangential displacements at the interface scale with the fiber radius whereas the critical values for these relative displacements l_{Nc} and l_{Tc} do not. As a consequence, $\sigma_{1c} \propto 1/a$ which corresponds to a quadratic curve in Figure 4. This means why the two models diverge necessarily for this limit.

5. Concluding remarks

A comparison has been carried out between the fiber-size effect predicted by a cohesive zone model and a finite fracture mechanics model for the problem of crack initiation at the fiber-matrix interface under transverse tension.

A good agreement between the two approaches has been noticed for a wide range of fiber diameters. The differences in the models predictions for very small and very large fibers is reasonable and the reasons for that have been interpreted according to two simplified asymptotic solutions.

Acknowledgements

This work was supported by the Spanish Ministry of Education (FPU grant 2009/3968), and Economy and Competitiveness (Project MAT2012-37387); the Junta de Andalucía and European Social Fund (Project TEP-04051). MP would like to thank the support of the Italian Ministry of Education, University and Research to the Project FIRB 2010 Future in Research Structural mechanics models for renewable energy applications (RBFR107AKG).

References

[1] F. París, E. Correa, and V. Mantič. Kinking of transversal interface cracks between fiber and matrix. *Journal of Applied Mechanics*, 74(4):703–716, 2007.

[2] A. Carpinteri, M. Paggi, and G. Zavarise. Snap-back instability in micro-structured composites and its connection with superplasticity. *Strength, Fracture and Complexity*, 3(2):61 – 72, 2005.

[3] V. Mantič. Interface crack onset at a circular cylindrical inclusion under a remote transverse tension. Application of a coupled stress and energy criterion. *International Journal of Solids and Structures*, 46(6):1287 – 1304, 2009.

[4] V.I. Kushch, S.V. Shmegera, P. Brøndsted, and L. Mishnaevsky. Numerical simulation of progressive debonding in fiber reinforced composite under transverse loading. *International Journal of Engineering Science*, 49(1):17–29, 2011.

[5] L. Távara, V. Mantič, E. Graciani, and F. París. BEM analysis of crack onset and propagation along fiber-matrix interface under transverse tension using a linear elastic-brittle interface model. *Engineering Analysis with Boundary Elements*, 35(2):207–222, 2011.

[6] D. Leguillon. Strength or toughness? A criterion for crack onset at a notch. *European Journal of Mechanics and Solids*, 21(1):61–72, 2002.

[7] Z. Hashin. Finite thermoelastic fracture criterion with application to laminate cracking analysis. *Journal of the Mechanics and Physics of Solids*, 44(7):1129–1145, 1996.

[8] P. Cornetti, N. Pugno, A. Carpinteri, and D. Taylor. Finite fracture mechanics: A coupled stress and energy failure criterion. *Engineering Fracture Mechanics*, 73(14):2021–2033, 2006.

[9] K. Park and G. H. Paulino. Cohesive zone models: A critical review of traction-separation relationships across fracture surfaces. *Applied Mechanics Reviews*, 64(6), 2011.

[10] I.G. García, M. Paggi, and V. Mantič. Fiber-size effects on the onset of fibermatrix debonding under transverse tension: A comparison between cohesive zone and finite fracture mechanics models. *Engineering Fracture Mechanics*, 115:96–110, 2014.

[11] V. Tvergaard. Analysis of tensile properties for a whisker-reinforced metal-matrix composite. *Acta Metallurgica Et Materialia*, 38(2):185–194, 1990.

[12] G. Zavarise, D. P. Boso, and B. A. Schrefler. A formulation for electrostatic-mechanical contact and its numerical solution. *International Journal of Numerical Methods in Engineering*, 64:382–400, 2005.

[13] A. Carpinteri, M. Paggi, and G. Zavarise. The effect of contact on the decohesion of laminated beams with multiple microcracks. *International Journal of Solids and Structures*, 45:129–143, 2008.

[14] J.N. Goodier. Concentration of stress around spherical and cylindrical inclusions and flaws. *Journal of Applied Mechanics*, 55:39–44, 1933.

[15] M. Toya. A crack along the interface of a rigid circular inclusion embedded in an elastic solid. *International Journal of Fracture*, 9(4):463–470, 1974.